Multiplexing/Beamforming Switching for Coded MIMO in Spatially Correlated Channels Based on Closed-Form BER Approximations

Matthew R. McKay, *Member, IEEE*, Iain B. Collings, *Senior Member, IEEE*, Antonio Forenza, *Member, IEEE*, and Robert W. Heath, Jr., *Senior Member, IEEE*

***Abstract*—This paper considers low-complexity coded multiple-input–multiple-output transmission in Rayleigh channels with correlation between antennas at both the transmitter and receiver. We consider statistical beamforming (SB) and spatial multiplexing (SM) with a zero-forcing receiver. We calculate the link-level capacity of both schemes with bit-interleaved coded modulation and derive accurate closed-form approximations to the bit error rate. We then show how the resulting expressions can be used in an adaptive algorithm to select the best combination of code rate, modulation format, and transmission scheme (SB or SM) in order to maximize throughput. Unlike other mode-switching schemes that require empirical lookup tables, this approach applies to any correlation scenario. Numerical studies are used to demonstrate the performance as a function of signal-to-noise ratio and correlation parameters.**

***Index Terms*—Adaptive coding, modulation, multiple-input–multiple-output (MIMO) communications, spatially correlated channels.**

I. Introduction

MULTIPLE-INPUT–MULTIPLE-OUTPUT (MIMO) antenna technology has emerged as an effective technique for increasing the capacity [1] and robustness [2] of wireless communications systems. An important characteristic of MIMO communication systems is the fundamental tradeoff between diversity gain and multiplexing gain, and this is currently a topic of considerable research. In [3], an information-theoretic treatment was given for independent identically distributed (i.i.d.) Rayleigh MIMO channels at high signal-to-noise ratio (SNR). In [4] and [5], practical techniques were designed to take advantage of this tradeoff by adaptively switching between diversity and multiplexing transmission modes in i.i.d. Rayleigh channels, depending on the channel state information. A similar method was also proposed in [6] for spatially correlated channels, which adaptively selected a combination of a transmit-antenna subset and modulation format, based on the channel spatial statistics. Compared with nonadaptive transmission, the preceding adaptive schemes were shown to yield significant gains in error performance for fixed data rate.

In this paper, we extend the scope of investigation by considering coded modulation over channels with correlation between antennas at *both* the transmitter and receiver (double ended), and we focus on maximizing the data rate for a given target error performance. For this broader more practical class of systems, we consider two simple MIMO schemes: 1) statistical beamforming (SB) and 2) spatial multiplexing (SM) with a zero-forcing (ZF) receiver. The former requires only covariance feedback information; the latter one is an open-loop scheme with a low-complexity linear receiver.

We consider the possibility of switching between these practical schemes in order to maximize system throughput. Of course, it is common to adapt between a set of coding and modulation modes based on SNR, e.g., as discussed in [7]. The key in this paper is to also introduce the possibility of adaptive switching between SB in high-correlation conditions and SM in low-correlation conditions. This switching method will improve the performance and requires minimal feedback information since it relies on only two channel statistics: 1) the average SNR and 2) the spatial correlation.

We start by deriving new accurate closed-form approximations to the bit error rate (BER) for both the SB and SM MIMO schemes. No previous closed-form BER results are known for these schemes when they have both double-ended correlation and coding. The coding that we consider is bit-interleaved coded modulation (BICM) [8], [9], which is common in practical wireless systems (e.g., IEEE 802.11a WLANs and proposed for IEEE 802.11n) and is ideally suited to adaptive transmission. BICM is easily adapted to changing channel conditions by simply puncturing the mother encoder and changing to a corresponding modulation format. Recently, BICM schemes have been extended to uncorrelated MIMO

Manuscript received January 17, 2006; revised July 27, 2006 and October 26, 2006. This work is supported in part by the National Science Foundation under Grant CNS-0435307 and Grant CCF-514194, by the Office of Naval Research under Grant N00014-05-1-0169, and by Freescale Semiconductor. This paper was presented in part at the IEEE International Conference on Communications, Istanbul, Turkey, June 2006. The review of this paper was coordinated by Dr. E. Larsson.

M. R. McKay is with the Department of Electronic and Computer Engineering, Hong Kong University of Science and Technology, Clear Water Bay, Kowloon, Hong Kong (e-mail: eemckay@ust.hk).

I. B. Collings is with the Wireless Technologies Laboratory, Information and Communication Technologies Centre, Commonwealth Scientific and Industrial Research Organisation, Marsfield, N.S.W. 2122, Australia (e-mail: iain.collings@csiro.au).

A. Forenza is with Rearden, LLC, San Francisco, CA 94107 USA (e-mail: antonio@rearden.com).

R. W. Heath, Jr. is with the Wireless Networking and Communications Group, Department of Electrical and Computer Engineering, University of Texas at Austin, TX 78712 USA (e-mail: rheath@ece.utexas.edu).

Color versions of one or more of the figures in this paper are available online at http://ieeexplore.ieee.org.

Digital Object Identifier 10.1109/TVT.2007.900353

scenarios, where they were shown to perform favorably in SM systems employing practical ZF receivers [10], [11].

Our derivations are based on the typical BICM assumption of ideal interleaving. This assumption is valid in channels with sufficient time variation or frequency selectivity. We make use of a saddlepoint approach (originally proposed in [12] and [13] for the single-input–single-output (SISO) BICM case) and employ a high-SNR analysis. The expressions can be used to approximate achievable throughputs for given combinations of coding and modulation.

We then show how the resulting BER approximations can be used to adaptively select the best combination of code rate, modulation format, and transmission scheme (SB or SM), in order to maximize throughput in the double-ended correlated channels. The only previous adaptive schemes for channels with both transmit and receive correlation, of which we know, are limited by the fact that the mode selection criterion is based on empirically generated lookup tables that were constructed from a small set of typical channel scenarios [14], [15] or are based on loose SNR approximations [6], thus making the switching inaccurate. We note that it may also be possible to get closed-form results for other more complicated receiver structures, such as minimum mean-square error (MMSE), successive interference cancellation, and maximum likelihood (ML) receivers, although this is beyond the scope of this paper. (In the particular case of the MMSE receiver, the performance is known to be close to ZF, and hence, the switching algorithm that we develop here could be applied directly with a small approximation error. In the case of ML, it has been previously shown that, with the particular codes that we consider in this paper, the performance is only marginally better than ZF when the modulation order or the number of receive antennas is high [10], [11].)

Finally, numerical studies, which demonstrate the throughput performance of the adaptive system in various correlation scenarios, are presented. These results confirm that adaptation achieves significant throughput improvements over nonadaptive systems while maintaining a predefined target BER. The results also demonstrate that an SM/SB switching system can perform close to the theoretical BICM link-level capacity (LLC) and that, by switching based on the closed-form BER approximations, near-optimal throughputs can be achieved for BER targets of practical interest.

II. System Description

A. System Model and Architecture

Consider a narrowband MIMO system with N_t and N_r transmit and receive antennas, respectively. Throughout this paper, we assume $N_t \leq N_r$ to facilitate low-complexity BICM–SM transmission (see the following). For each channel use, the received signal vector is given by

$$\mathbf{r} = \sqrt{\gamma}\,\mathbf{H}\mathbf{a} + \mathbf{n} \tag{1}$$

where $\mathbf{a} \in \mathcal{C}^{N_t \times 1}$ is the transmit signal vector satisfying the power constraint $E[\mathbf{a}^\dagger \mathbf{a}] = N_t$, and $\mathbf{n} \in \mathcal{C}^{N_r \times 1}$ is the noise vector $\sim \mathcal{CN}(\mathbf{0}_{N_r \times 1}, \mathbf{I}_{N_r})$. In addition, $\mathbf{H} \in \mathcal{C}^{N_r \times N_t}$ is the spatially correlated Rayleigh fading channel matrix, which is assumed to be known perfectly at the receiver, and γ is the average SNR per transmit antenna. The channel is decomposed according to the common Kronecker structure (as in [16]–[18], among others) as follows:

$$\mathbf{H} = \mathbf{R}^{\frac{1}{2}} \mathbf{H}_w \mathbf{S}^{\frac{1}{2}} \tag{2}$$

where $\mathbf{H}_w \in \mathcal{C}^{N_r \times N_t}$ contains independent entries $H_{i,j} \sim \mathcal{CN}(0,1)$, and $\mathbf{R} \in \mathcal{C}^{N_r \times Nr}$ and $\mathbf{S} \in \mathcal{C}^{N_t \times N_t}$ are the receive and transmit-correlation matrices with eigenvalue decompositions

$$\mathbf{R} = \mathbf{U}_r \mathbf{\Lambda}_r \mathbf{U}_r^\dagger \quad \mathbf{S} = \mathbf{U}_s \mathbf{\Lambda}_s \mathbf{U}_s^\dagger. \tag{3}$$

We assume that $\mathbf{R}$ and $\mathbf{S}$ are Hermitian positive-definite matrices containing unit diagonal entries. Moreover, we assume that the eigenvector $\mathbf{u}_{s,\max}$ corresponding to the maximum eigenvalue of $\mathbf{S}$ is known perfectly at the transmitter (this is to facilitate SB; see the following). With this model, the average SNR per receive antenna is $N_t\gamma$.

Note that all analytical results presented in this paper apply equally to any particular correlation model that can be expressed in the form of (2). For the numerical studies that we consider, the exponential correlation model at the transmitter and receiver (e.g., as in [17]) is given by

$$\mathbf{R}_{i,j} = \rho_{\mathrm{rx}}^{|i-j|} \quad \mathbf{S}_{i,j} = \rho_{\mathrm{tx}}^{|i-j|} \tag{4}$$

where ρ_{rx} and ρ_{tx} are the receive and transmit spatial correlation coefficients between adjacent antennas. We choose this simple exponential correlation model (for the numerical studies) to illustrate clearly the impact of correlation on the relative performance of the SB and SM schemes. Other more sophisticated correlation models could be also considered.

The MIMO system architecture that we analyze is presented in Fig. 1. The encoder, interleaver (assumed ideal), and constellation mapper form the BICM section of the transmitter. The BICM system operates according to one of a finite set of modes, with each mode comprising a particular combination of encoder rate and modulation format (hereafter denoted as the BICM mode). Encoder rate R is varied by puncturing a mother binary convolutional encoder. The modulation formats are Gray-labeled 2^M-ary phase-shift keying (PSK) or quadratic amplitude modulation (QAM) constellations, which is denoted $\mathcal{A}$, of unit average energy. Following modulation, the symbols are mapped to transmit signal vectors $\mathbf{a}$, according to the particular MIMO transmission scheme, as discussed in the following section.

B. Low-Complexity MIMO Transmission Schemes

This section details an SB scheme, which will be shown to be suited to channels with high correlation or low SNR, and an SM scheme, which will be shown to perform best in uncorrelated channels and high SNR.

1) SB: For the SB scheme, a single modulated symbol is transmitted from all the antennas, with an appropriate complex

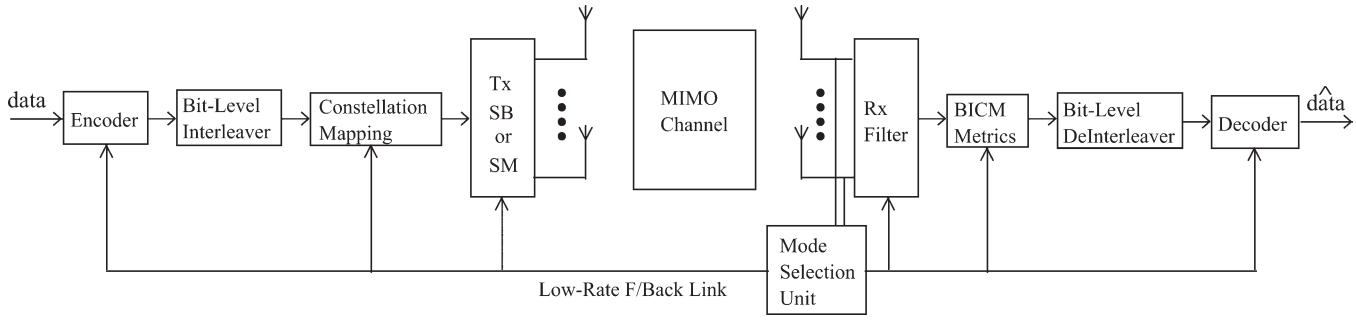

Fig. 1. MIMO BICM system architecture.

weighting, during each channel use. For a modulated symbol $a \in \mathcal{A}$, the transmission vector $\mathbf{a}$ is formed as follows:

$$\mathbf{a} = \mathbf{u}_{s,\max} a. \tag{5}$$

The spectral efficiency of BICM–SB, in bits per second per hertz, is therefore

$$S_{\mathrm{BICM-SB}} = RM. \tag{6}$$

2) SM: For the SM scheme, N_t modulated symbols are transmitted, one per antenna, during each channel use. The spectral efficiency of BICM–SM, in bits per second per hertz, is therefore given by

$$S_{\mathrm{BICM-SM}} = N_t RM. \tag{7}$$

Clearly, for a given mode (R and M), $S_{\mathrm{BICM-SM}}$ is larger than $S_{\mathrm{BICM-SB}}$ by a factor of N_t.

C. Low-Complexity MIMO BICM Receivers

1) SB: For the SB scheme, maximum ratio combining is applied to the receive signal vector to yield

$$\begin{aligned} z &= \mathbf{f}^\dagger \mathbf{r} = \sqrt{\gamma}\mathbf{f}^\dagger(\mathbf{H}\mathbf{u}_{\mathrm{s,max}} a + \mathbf{n}) \\ &= \sqrt{\gamma}\|\mathbf{f}\|^2 a + \underline{n} \end{aligned} \tag{8}$$

where $\mathbf{f} = \mathbf{H}\mathbf{u}_{s,\max}$, and $\underline{n} = \mathbf{f}^\dagger \mathbf{n} \sim \mathcal{CN}(0, \|\mathbf{f}\|^2)$. The BICM log-likelihood metrics for each of the bits $i(= 1, \ldots, M)$ corresponding to the modulated symbol a are calculated from z using

$$\mathcal{L}_i = \ln \frac{\sum_{\tilde{a} \in \mathcal{A}_1^i} p(z|\tilde{a}, \mathbf{f})}{\sum_{\tilde{a} \in \mathcal{A}_0^i} p(z|\tilde{a}, \mathbf{f})} \tag{9}$$

where

$$p(z|\tilde{a}, \mathbf{f}) = \frac{1}{\pi\|\mathbf{f}\|^2} \exp\left(-\frac{|z - \sqrt{\gamma}\|\mathbf{f}\|^2 \tilde{a}|^2}{\|\mathbf{f}\|^2}\right) \tag{10}$$

and where $\mathcal{A}_0^i, \mathcal{A}_1^i$ are the signal subsets within $\mathcal{A}$, with the ith bit being equal to 0 and 1, respectively. These metrics are deinterleaved and decoded using a soft-decision Viterbi algorithm.

2) SM: For the SM scheme, the initial filtering step at the receiver is

$$\mathbf{z} = \mathbf{W}\mathbf{r} = \sqrt{\gamma}\mathbf{a} + \underline{\mathbf{n}} \tag{11}$$

where $\mathbf{W} = (\mathbf{H}^\dagger\mathbf{H})^{-1}\mathbf{H}^\dagger$, and $\underline{\mathbf{n}} = \mathbf{W}\mathbf{n} \sim \mathcal{CN}(\mathbf{0}_{N_t \times 1}, \mathbf{W}\mathbf{W}^\dagger)$. Clearly, the kth element of $\mathbf{z}$ corresponds to the output from a colored Gaussian noise channel, where the input is the kth element of $\mathbf{a}$. For the kth modulated symbol a_k, the BICM log-likelihood metrics are then calculated for the corresponding bits $i(= 1, \ldots, M)$ according to [10], [11]

$$\mathcal{L}_{k,i} = \ln \frac{\sum_{\tilde{a} \in \mathcal{A}_1^i} p(z_k|\tilde{a}, \mathbf{w}_k)}{\sum_{\tilde{a} \in \mathcal{A}_0^i} p(z_k|\tilde{a}, \mathbf{w}_k)} \tag{12}$$

where z_k is the kth element of $\mathbf{z}$, $\mathbf{w}_k$ is the kth row vector of $\mathbf{W}$, and

$$p(z_k|\tilde{a}, \mathbf{w}_k) = \frac{1}{\pi\|\mathbf{w}_k\|^2} \exp\left(-\frac{|z_k - \sqrt{\gamma}\tilde{a}|^2}{\|\mathbf{w}_k\|^2}\right). \tag{13}$$

These metrics are deinterleaved and decoded using a soft-decision Viterbi algorithm.

III. Information Theoretic Analysis

In this section, we calculate and compare the BICM–SB and BICM–SM LLCs in spatially correlated Rayleigh MIMO channels. Assuming uniformly distributed inputs and ideal interleaving, the LLC is calculated by summing the mutual information for each equivalent BICM subchannel (i.e., as in [9] and [11]).[1]

A. LLC of MIMO BICM With SB (BICM–SB)

Using a technique for the LLC of SISO–BICM from [9], we obtain the LLC of BICM–SB as

$$C_{\mathrm{BICM\_SB}} = M - \sum_{i=1}^{M} E_{u,z,\mathbf{f}}\left[\log_2 \frac{\sum_{\tilde{a} \in \mathcal{A}} p(z|\tilde{a}, \mathbf{f})}{\sum_{\tilde{a} \in \mathcal{A}_u^i} p(z|\tilde{a}, \mathbf{f})}\right] \tag{14}$$

where u is an equivalent-channel binary input taking values of 0 and 1 with equal probability, independent of z and $\mathbf{f}$. Substituting the conditional probability density function (pdf)

[1]For general MIMO capacity analysis (Gaussian inputs), see [1], [16], [18], and [19].

(10) and using (8), we average over u and the uniformly distributed channel inputs $a \in \mathcal{A}_u^i$ to obtain

$$C_{\mathrm{BICM\_SB}} = M - \frac{1}{2^M}\sum_{i=1}^{M}\sum_{u=0}^{1}\sum_{a\in\mathcal{A}_u^i} \times E_{n,\mathbf{f}}\left[\log_2 \frac{\sum_{\tilde{a}\in\mathcal{A}} \exp\left(-\frac{\left|\sqrt{\gamma}\|\mathbf{f}\|^2(a-\tilde{a})+n\right|^2}{\|\mathbf{f}\|^2}\right)}{\sum_{\tilde{a}\in\mathcal{A}_u^i} \exp\left(-\frac{\left|\sqrt{\gamma}\|\mathbf{f}\|^2(a-\tilde{a})+n\right|^2}{\|\mathbf{f}\|^2}\right)}\right]. \quad (15)$$

In Section V, we present a closed-form expression for the pdf of $\|\mathbf{f}\|^2$. Using this pdf and the usual Gaussian pdf for n, the expectations in (15) can be efficiently computed using a combination of Gauss–Laguerre and Gauss–Hermite quadratures, which are tabulated in [20].

B. LLC of MIMO BICM With SM (BICM–SM)

We have previously derived the LLC for BICM–SM in i.i.d. Rayleigh channels as [11]

$$C_{\mathrm{BICM\_SM}} = MN_t - \sum_{k=1}^{N_t}\sum_{i=1}^{M} E_{u,z_k,\mathbf{w}_k}\left[\log_2 \frac{\sum_{\tilde{a}\in\mathcal{A}} p(z_k|\tilde{a},\mathbf{w}_k)}{\sum_{\tilde{a}\in\mathcal{A}_u^i} p(z_k|\tilde{a},\mathbf{w}_k)}\right] \quad (16)$$

where u is distributed as in (14). We note that this expression applies equally to spatially correlated channels, under the assumption of ideal interleaving. Substituting the conditional pdf (13) into (16), using (11), and averaging over u and $a \in \mathcal{A}_u^i$, we obtain

$$C_{\mathrm{BICM\_SM}} = MN_t - \frac{1}{2^M}\sum_{k=1}^{N_t}\sum_{i=1}^{M}\sum_{u=0}^{1}\sum_{a\in\mathcal{A}_u^i} \times E_{\underline{n}_k,\mathbf{w}_k}\left[\log_2 \frac{\sum_{\tilde{a}\in\mathcal{A}} \exp\left(-\frac{\left|\sqrt{\gamma}(a-\tilde{a})+\underline{n}_k\right|^2}{\|\mathbf{w}_k\|^2}\right)}{\sum_{\tilde{a}\in\mathcal{A}_u^i} \exp\left(-\frac{\left|\sqrt{\gamma}(a-\tilde{a})+\underline{n}_k\right|^2}{\|\mathbf{w}_k\|^2}\right)}\right]. \quad (17)$$

For transmit-correlated channels, the pdf of $\|\mathbf{w}_k\|^{-2}$ is known in closed form [21], and the expectations in (17) can be computed efficiently using Gauss–Laguerre and Gauss–Hermite quadratures. For channels with both transmit and receive correlations, such closed-form pdfs are not available, and the expectations must be evaluated through simulation.

C. LLC Performance Comparison

Fig. 2 compares the LLCs of BICM–SB and BICM–SM with 2×2 antennas for two correlation scenarios. Each curve is the envelope of the individual LLC curves for Gray-labeled binary PSK, quaternary PSK, 16QAM, and 64QAM modulation formats (for the respective transmission scheme).

The figure shows that the LLC of each transmission scheme depends on the channel correlation scenario. In particular, as the transmit correlation increases, SB benefits, and SM degrades. These curves motivate our new adaptive transmission approach,

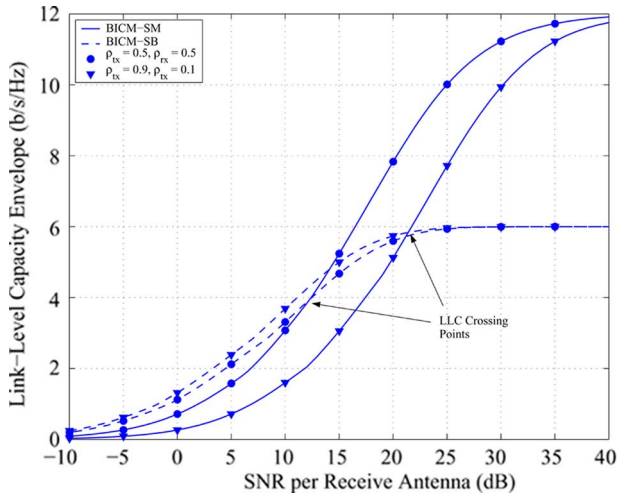

Fig. 2. BICM LLC envelope for the SM and SB transmission schemes. Two MIMO channel scenarios with exponential correlation coefficients $\rho_{\mathrm{tx}} = 0.5, \rho_{\mathrm{rx}} = 0.5$ and $\rho_{\mathrm{tx}} = 0.9, \rho_{\mathrm{rx}} = 0.1$ are considered.

which not only adapts the modulation format and code rate but also adapts the transmission scheme (between SB and SM). The relative performance of the two schemes clearly depends on both SNR and channel spatial correlation. For example, in the figure shown, in order to achieve the maximum LLC for the lower transmit-correlation channel, SB should be used for SNRs of below 12 dB, and SM should be used for higher SNRs. For the higher transmit-correlation channel, the crossing point is at 21 dB.

While these capacity results have motivated the new adaptive approach, for practical systems (with noncapacity-achieving codes), we prefer to evaluate the switching points based on achievable BER. Such is the topic of the following sections. In the numerical studies of Section VII-C, the capacity curves of this section are used as a benchmark of achievable performance.

IV. General Expressions for the Error Probability

We now derive tight expressions for the BER of BICM–SB and BICM–SM in spatially correlated Rayleigh MIMO channels. These results will provide the fundamental tools for establishing the selection criterion for our proposed adaptive MIMO BICM algorithm in Section VII.

Before proceeding, we note that, although we are considering binary convolutional codes with low-complexity Viterbi decoding, the subsequent analytical BER results also apply directly to BICM–SB and BICM–SM systems employing more powerful *turbolike* codes [12], [13], [22] with iterative decoding (e.g., serial/parallel concatenated codes, and repeat and accumulate codes) in the region beyond the waterfall threshold. It is only necessary to know the distance spectrum of the code. Moreover, the analytical procedure could also be adapted to BICM–SB and BICM–SM systems with iterative demodulation (ID) and non-Gray labelings (i.e., as in the BICM–ID systems considered in [23]–[25]). However, in these particular cases, the general BER union-bound approach that is used in the sequel is known to yield accurate results only in the error-floor

region of the BER curve (see, for example, [12], [13], and [24]). It is also important to emphasize that both turbolike codes and BICM–ID have much higher complexity than the noniterative schemes considered in this paper, making them unsuitable for implementation in many practical systems.

A. BER Union Bound

The BER union bound for rate $R = k_c/n_c$ linear binary convolutional codes is given by [26]

$$\text{BER} \leq \frac{1}{k_c} \sum_{d=d_{\text{free}}}^{\infty} W_I(d) f(d, \mu, \mathcal{A}, \gamma) \tag{18}$$

where $W_I(d)$ is the total input weight of all error events at Hamming distance d, $f(.)$ is the codeword pairwise error probability (C-PEP), μ is the labeling map, and d_{free} is the free Hamming distance. Note that, for the codes that we consider, the infinite series in (18) converges very quickly, and truncation to as little as five terms still yields accurate results.

B. Exact Expression for the C-PEP

To simplify the C-PEP analysis of both BICM–SB and BICM–SM, we adopt the approach of [9] and force the BICM subchannels[2] to behave as binary-input–output-symmetric channels by introducing a random bit-swapping variable u, which gives the well-known C-PEP [26]

$$f(d, \mu, \mathcal{A}, \gamma) = \Pr\left(\sum_{i=1}^{d} \mathcal{L}_i > 0\right) \tag{19}$$

assuming that the all-zero codeword is transmitted, and where $\mathcal{L}_i$ is the log-likelihood metric for the ith coded bit. Since the metrics $\mathcal{L}_i$ are i.i.d. under the assumption of ideal interleaving, we can evaluate the tail probability (19) based on the moment-generating function (mgf)[3]

$$\mathcal{M}_{\mathcal{L}}(s) \triangleq E_{\mathcal{L}}\left[\exp(s\mathcal{L})\right] \tag{20}$$

as

$$f(d, \mu, \mathcal{A}, \gamma) = \frac{1}{2\pi j} \int_{c-j\infty}^{c+j\infty} \mathcal{M}_{\mathcal{L}}(s)^d \frac{ds}{s}. \tag{21}$$

Unfortunately, in virtually all cases, this solution must be evaluated using numerical complex integration techniques, thereby making it unsuitable for use in practical adaptive systems. In this paper, we use (21) for assessing the accuracy of our efficient C-PEP closed-form approximations.

[2]These are the equivalent channels between the transmitted binary codeword and the corresponding BICM bit metrics.

[3]Note that we drop the subscript on $\mathcal{L}$ when considering the log-likelihood ratio statistics at a single instant in time.

C. Saddlepoint Approximation for the C-PEP

Since the C-PEP is the tail probability of a sum of i.i.d. random variables, a simplified closed-form expression is obtained by applying a saddlepoint approximation [27, App. 5A] to (19). This approximation is more accurate than the usual Chernoff bound and is given by

$$\begin{aligned} f(d, \mu, \mathcal{A}, \gamma) &\approx \frac{1}{\sqrt{2\pi d \mathcal{K}''_{\mathcal{L}}(\hat{s})}\hat{s}} \exp\left(d\mathcal{K}_{\mathcal{L}}(\hat{s})\right) \\ &= \frac{1}{\sqrt{2\pi d \mathcal{K}''_{\mathcal{L}}(\hat{s})}\hat{s}} \mathcal{M}_{\mathcal{L}}(\hat{s})^d \end{aligned} \tag{22}$$

where $\mathcal{K}_{\mathcal{L}}(\cdot)$ is the cumulant-generating function of $\mathcal{L}$ given by

$$\mathcal{K}_{\mathcal{L}}(s) = \ln \mathcal{M}_{\mathcal{L}}(s) \tag{23}$$

and where $\mathcal{K}''_{\mathcal{L}}(\hat{s})$ denotes the second derivative of $\mathcal{K}_{\mathcal{L}}(s)$, which is evaluated at the *saddlepoint* $\hat{s}$, which is the real value of s that minimizes $\mathcal{K}_{\mathcal{L}}(s)$ [and therefore also minimizes $\mathcal{M}_{\mathcal{L}}(s)$].

We note that the general saddlepoint approximation (22) was first used for the analysis of SISO BICM in AWGN and uncorrelated Rayleigh fading in [12] and further elaborated upon in [13]. In this paper, we apply the saddlepoint approximation to the more general correlated MIMO channel and use it to derive new closed-form approximations to the BER.

V. Performance Analysis of MIMO BICM With SB

A. MGF of Log-Likelihood Metric

For BICM–SB transmission, the mgf is easily obtained using (9), (10), and (20) as

$$\begin{aligned} \mathcal{M}_{\mathcal{L}}(s) &= E_{z,m,u,\mathbf{f}}\left[\exp\left(s \ln \frac{\sum_{\tilde{a}\in\mathcal{A}_{\bar{u}}^m} \exp\left(-\frac{\left|z-\sqrt{\gamma}\|\mathbf{f}\|^2\tilde{a}\right|^2}{\|\mathbf{f}\|^2}\right)}{\sum_{\tilde{a}\in\mathcal{A}_{u}^m} \exp\left(-\frac{\left|z-\sqrt{\gamma}\|\mathbf{f}\|^2\tilde{a}\right|^2}{\|\mathbf{f}\|^2}\right)}\right)\right] \\ &= E_{a,m,u,\underline{n},\mathbf{f}}\left[\left(\frac{\sum_{\tilde{a}\in\mathcal{A}_{\bar{u}}^m} \exp\left(-\frac{\left|\sqrt{\gamma}\|\mathbf{f}\|^2(a-\tilde{a})+\underline{n}\right|^2}{\|\mathbf{f}\|^2}\right)}{\sum_{\tilde{a}\in\mathcal{A}_{u}^m} \exp\left(-\frac{\left|\sqrt{\gamma}\|\mathbf{f}\|^2(a-\tilde{a})+\underline{n}\right|^2}{\|\mathbf{f}\|^2}\right)}\right)^s\right]. \end{aligned} \tag{24}$$

Averaging over the uniform bit positions m, bit-swapping values u, and symbols $a \in \mathcal{A}_u^m$ gives

$$\mathcal{M}_{\mathcal{L}}(s) = \frac{1}{M2^M} \sum_{m=1}^{M} \sum_{u=0}^{1} \sum_{a\in\mathcal{A}_u^m} \mathcal{I}_{m,u,a}(s) \tag{25}$$

where

$$\mathcal{I}_{m,u,a}(s) = E_{\underline{n},\mathbf{f}}\left[\left(\frac{\sum_{\tilde{a}\in\mathcal{A}_{\bar{u}}^m} \exp\left(-\frac{\left|\sqrt{\gamma}\|\mathbf{f}\|^2(a-\tilde{a})+\underline{n}\right|^2}{\|\mathbf{f}\|^2}\right)}{\sum_{\tilde{a}\in\mathcal{A}_{u}^m} \exp\left(-\frac{\left|\sqrt{\gamma}\|\mathbf{f}\|^2(a-\tilde{a})+\underline{n}\right|^2}{\|\mathbf{f}\|^2}\right)}\right)^s\right]. \tag{26}$$

As for the BICM–SB LLC in (15), the expectation (26) can be evaluated via numerical integration using Gauss–Laguerre and Gauss–Hermite quadratures. We now show that, at high SNR, the expression can be calculated in closed form. At high SNR, the ratio in (26) is dominated by a single minimum distance term[4] in the numerator and denominator, and by applying the bounding approach from [13, eq. 39], the Dominated Convergence Theorem [28] can be applied. For the remainder of the section, we assume a high-SNR scenario and have

$$\mathcal{I}_{m,u,a}(s) = E_{\underline{n},\mathbf{f}}\left[\left(\frac{\exp\left(-\frac{\left|\sqrt{\gamma}\|\mathbf{f}\|^2(a-\tilde{a})+\underline{n}\right|^2}{\|\mathbf{f}\|^2}\right)}{\exp\left(-\frac{|\underline{n}|^2}{\|\mathbf{f}\|^2}\right)}\right)^s\right] \tag{27}$$

for $s<1$, where $\tilde{a}\in\mathcal{A}_u^m$ is the nearest neighbor to $a\in\mathcal{A}_u^m$. Averaging over the noise yields

$$\begin{aligned}
&\mathcal{I}_{m,u,a}(s)\\
&\quad= E_{\underline{n},\mathbf{f}}\left[\exp\left(\frac{-s\left|\sqrt{\gamma}\|\mathbf{f}\|^2(a-\tilde{a})+\underline{n}\right|^2+s|\underline{n}|^2}{\|\mathbf{f}\|^2}\right)\right]\\
&\quad= E_{\underline{n},\mathbf{f}}\left[\exp\left(\frac{-s\gamma\|\mathbf{f}\|^4|a-\tilde{a}|^2-2s\Re\mathrm{e}\left(\sqrt{\gamma}\|\mathbf{f}\|^2(a-\tilde{a})\underline{n}^*\right)}{\|\mathbf{f}\|^2}\right)\right]\\
&\quad= E_{\mathbf{f}}\Bigg[\exp\left(-s\gamma\|\mathbf{f}\|^2|a-\tilde{a}|^2+s^2\gamma\|\mathbf{f}\|^2|a-\tilde{a}|^2\right)\\
&\qquad\times\int\frac{1}{\pi}\exp\left(-\frac{\left|\underline{n}+s\sqrt{\gamma}\|\mathbf{f}\|^2(a-\tilde{a})\right|^2}{\|\mathbf{f}\|^2}\right)d\underline{n}\Bigg]\\
&\quad= E_{\|\mathbf{f}\|^2}\left[\exp\left(-\gamma\|\mathbf{f}\|^2|a-\tilde{a}|^2s(1-s)\right)\right].
\end{aligned} \tag{28}$$

To evaluate the expectation in (28), we use (2) and (3) and recall that the distribution of $\mathbf{H}_w$ in (2) is invariant under unitary transformation to give

$$\begin{aligned}
\|\mathbf{f}\|^2 &= \mathbf{u}_{s,\max}^\dagger\mathbf{H}^\dagger\mathbf{H}\mathbf{u}_{s,\max}\\
&\simeq \mathbf{u}_{s,\max}^\dagger\mathbf{U}_s\mathbf{\Lambda}_s^{\frac{1}{2}}\mathbf{U}_s^\dagger\mathbf{H}_w^\dagger\mathbf{U}_r\mathbf{\Lambda}_r\mathbf{U}_r^\dagger\mathbf{H}_w\mathbf{U}_s\mathbf{\Lambda}_s^{\frac{1}{2}}\mathbf{U}_s^\dagger\mathbf{u}_{s,\max}\\
&\simeq \mathbf{u}_{s,\max}^\dagger\mathbf{U}_s\mathbf{\Lambda}_s^{\frac{1}{2}}\mathbf{H}_w^\dagger\mathbf{\Lambda}_r\mathbf{H}_w\mathbf{\Lambda}_s^{\frac{1}{2}}\mathbf{U}_s^\dagger\mathbf{u}_{s,\max}\\
&\simeq \frac{\lambda_{s,\max}}{2}\mathcal{Q}
\end{aligned} \tag{29}$$

where $\simeq$ denotes equivalence in distribution, $\lambda_{s,\max}$ is the maximum eigenvalue of $\mathbf{S}$, and

$$\mathcal{Q} = \sum_{\ell=1}^{N_r}\varepsilon_\ell\lambda_{r,\ell} \tag{30}$$

where $\lambda_{r,\ell}$ denotes the ℓth eigenvalue of $\mathbf{R}$, and the ε_ℓ's are i.i.d. exponentially distributed random variables. As such, $\mathcal{Q}$ is a central quadratic form. Since the exponential distribution is a chi-squared distribution with *even* degrees of freedom, we use a general result from [29] to give the pdf of $\mathcal{Q}$ as

$$f(\mathcal{Q}) = \sum_{\ell=1}^{N_r} g_\ell(\mathbf{\Lambda}_r)\frac{\exp\left(-\frac{\mathcal{Q}}{2\lambda_{r,\ell}}\right)}{2\lambda_{r,\ell}} \tag{31}$$

where

$$g_\ell(\mathbf{\Lambda}_r) = \prod_{j=1,j\neq\ell}^{N_r}\left(\frac{\lambda_{r,\ell}}{\lambda_{r,\ell}-\lambda_{r,j}}\right). \tag{32}$$

Using (31) and (29), along with the integration identity [30, eq. (3.381.4)], the expectation in (28) is evaluated as

$$\mathcal{I}_{m,u,a}(s) = \sum_{\ell=1}^{N_r} g_\ell(\mathbf{\Lambda}_r)\left(1+\gamma|a-\tilde{a}|^2\lambda_{s,\max}\lambda_{r,\ell}s(1-s)\right)^{-1}. \tag{33}$$

Now, substituting (33) into (25) gives a closed-form expression for the mgf. Unfortunately, this expression requires the calculation of $M2^MN_t$ terms, i.e., $\mathcal{I}_{m,u,a}(s)$. We can see from (25), however, that these terms only depend on a through the squared Euclidean distance to its nearest neighbor $\tilde{a}$ in the complement subset. We previously showed in [31] that, when Gray-labeling PSK/QAM constellations were employed, summations of this form could be greatly simplified by exploiting the multiplicities of the Euclidean distances. In particular, in this case, we find that (25) can be written in the efficient form

$$\mathcal{M}_{\mathcal{L}}(s) = \sum_{i=1}^{|P_M|}\mathcal{P}_{M,i}\hat{\mathcal{I}}_{\mathcal{E}_{M,i}}(s) \tag{34}$$

where the sets $\mathcal{P}_M$ (with cardinality $|\mathcal{P}_M|$) and $\mathcal{E}_M$ are defined in Table I, with the ith element $\mathcal{P}_{M,i}$ and $\mathcal{E}_{M,i}$, respectively, and $\hat{\mathcal{I}}_{\mathcal{E}_{M,i}}(s)$ is as in (33) but with $|a-\tilde{a}|^2$ replaced with $\mathcal{E}_{M,i}$.

TABLE I
BREAKDOWN OF DISTANCE MULTIPLICITIES BETWEEN COMPLEMENT BICM SUBSETS FOR VARIOUS GRAY-LABELED CONSTELLATIONS

	$\mathcal{P}_M$	$\mathcal{E}_M$
BPSK	{1}	{4.0}
QPSK	{1}	{2.0}
16QAM	{3/4, 1/4}	{0.4, 1.6}
64QAM	{7/12, 1/4, 1/12, 1/12}	{0.0952, 0.3810, 0.8571, 1.5238}

B. Closed-Form C-PEP Based on Saddlepoint Approximation

Noting that the mgf (34) is minimized at the saddlepoint $\hat{s}=1/2$, we use (34) in (22) to obtain (after simple but tedious algebra) the saddlepoint approximation to the C-PEP that is given in (35), shown at the bottom of the next page.

This expression is easy to compute in practice since $|\mathcal{P}_M|$ is small, and all terms are straightforward functions of the eigenvalues of the correlation matrices and the SNR.

[4]Note that if non-Gray mappings were considered, the multiplicity of nearest neighbors would need to be considered.

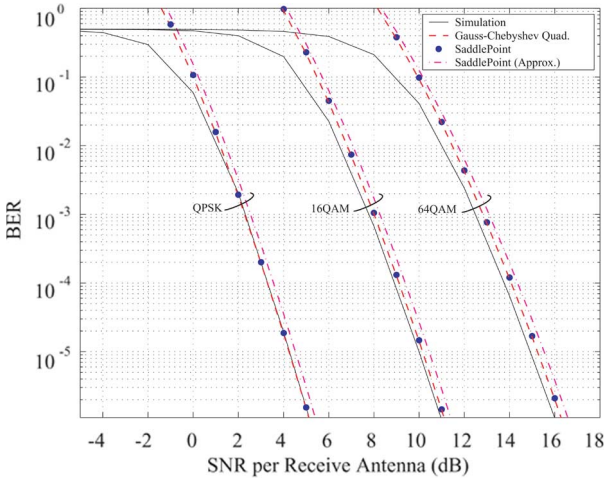

Fig. 3. Simulated and analytical BER for 2 × 2 BICM–SB with a 1/2-rate code and for various modulation schemes. An exponential correlation model is used, with a correlation coefficient of 0.5 at both the transmitter and receiver.

C. Simplified C-PEP

Applying the following approximation to the denominator of (35):

$$\left(\frac{\gamma\mathcal{E}_{M,i}\lambda_{s,\max}\lambda_{r,\ell}}{4}\right) \approx \left(\frac{\gamma\mathcal{E}_{M,i}\lambda_{s,\max}\lambda_{r,\ell}}{4}\right) + 1 \qquad (36)$$

we obtain a simplified C-PEP expression that is given by

$$f(d,\mu,\mathcal{A},\gamma) \approx \frac{1}{2\sqrt{\pi d}}\left[\sum_{i=1}^{|\mathcal{P}_M|}\mathcal{P}_{M,i}\sum_{\ell=1}^{N_r} g_\ell(\mathbf{\Lambda}_r) \times \left(1+\frac{\gamma\mathcal{E}_{M,i}\lambda_{s,\max}\lambda_{r,\ell}}{4}\right)^{-1}\right]^d. \qquad (37)$$

D. BER Performance Results

Fig. 3 compares the preceding analytical BICM–SB BER expressions with Monte Carlo simulation results, for a 2 × 2 system with Gray-labeled QPSK, 16QAM, and 64QAM constellations. Results are presented for the optimal 64-state 1/2-rate binary convolutional code with $d_{\text{free}} = 10$ and with ideal interleaving. We consider the exponential correlation model with correlation coefficients $\rho_{\text{tx}} = \rho_{\text{rx}} = 0.5$. The "saddlepoint" curves were obtained by substituting the C-PEP expression (35) into (18). Note that, as expected, they are within 0.2 dB of the simulated curves for low to moderate BERs since the union bound is known to be tight for convolutional codes for SNRs above the cutoff rate. The "saddlepoint (approx)" curves were obtained from (37) and are within 1 dB of the simulated curves in all cases. For comparison, results are also presented based on the exact C-PEP expression (21). To evaluate this expression, the mgf (34) was used in (21), and the complex integration was evaluated numerically using Gauss–Chebyshev quadrature (GCQ) rules [32]. We clearly see that the simplified closed-form saddlepoint approximation suffers negligible loss compared with (21).

VI. Performance Analysis of MIMO BICM With SM

A. MGF of Log-Likelihood Metric

For BICM–SM transmission, the mgf is easily obtained using (12), (13), and (20) as

$$\mathcal{M}_{\mathcal{L}}(s) = E_{z,m,u,k,\mathbf{w}_k}\left[\exp\left(s\ln\frac{\sum_{\tilde{a}\in\mathcal{A}_u^m}\exp\left(-\frac{|z-\sqrt{\gamma}\tilde{a}|^2}{|\mathbf{w}_k|^2}\right)}{\sum_{\tilde{a}\in\mathcal{A}_u^m}\exp\left(-\frac{|z-\sqrt{\gamma}\tilde{a}|^2}{|\mathbf{w}_k|^2}\right)}\right)\right]. \qquad (38)$$

In [31], we presented a closed-form high-SNR solution to (38) given by

$$\mathcal{M}_{\mathcal{L}}(s) = \frac{1}{N_t}\sum_{k=1}^{N_t}\sum_{i=1}^{|P_M|}\mathcal{P}_{M,i}\tilde{\mathcal{I}}_{k,\mathcal{E}_{M,i}}(s) \qquad (39)$$

where

$$\tilde{\mathcal{I}}_{k,\mathcal{E}_{M,i}}(s) \approx \left|\mathbf{I}_{N_r} + \frac{\gamma\mathcal{E}_{M,i}s(1-s)\mathbf{\Lambda}_r}{[\mathbf{S}^{-1}]_{k,k}}\right|^{-1} \underline{\text{tr}}_{N_t-1}(\mathbf{\Lambda}_r) \times \text{tr}_{N_t-1}\left(\mathbf{\Lambda}_r\left[\mathbf{I}_{N_r}+\frac{\gamma\mathcal{E}_{M,i}s(1-s)\mathbf{\Lambda}_r}{[\mathbf{S}^{-1}]_{k,k}}\right]^{-1}\right) \qquad (40)$$

where $[\cdot]_{k,k}$ denotes the kth diagonal element, and $\text{tr}_\ell(\cdot)$ is the ℓth elementary symmetric function, which is defined as [33], [34]

$$\text{tr}_\ell(\mathbf{X}) = \sum_{\{\underline{\alpha}\}}\prod_{i=1}^{\ell}\lambda_{x,\alpha_i} = \sum_{\{\underline{\alpha}\}}|\mathbf{X}_{\underline{\alpha}}^{\underline{\alpha}}| \qquad (41)$$

for arbitrary Hermitian positive-definite $\mathbf{X} \in \mathcal{C}^{n\times n}$. In (41), the sum is over all ordered $\underline{\alpha} = \{\alpha_1,\ldots,\alpha_\ell\} \subseteq \{1,\ldots,n\}$, $\lambda_{x,i}$ denotes the ith eigenvalue of $\mathbf{X}$, and $\mathbf{X}_{\underline{\alpha}}^{\underline{\alpha}}$ is the $\ell\times\ell$ principle submatrix of $\mathbf{X}$, which is formed by taking only the rows and columns that are indexed by $\underline{\alpha}$.

$$f(d,\mu,\mathcal{A},\gamma) \approx \frac{1}{2\sqrt{\pi d}}\frac{\left[\sum_{i=1}^{|\mathcal{P}_M|}\mathcal{P}_{M,i}\sum_{\ell=1}^{N_r} g_\ell(\mathbf{\Lambda}_r)\left(1+\frac{\gamma\mathcal{E}_{M,i}\lambda_{s,\max}\lambda_{r,\ell}}{4}\right)^{-1}\right]^{d+\frac{1}{2}}}{\sqrt{\sum_{i=1}^{|\mathcal{P}_M|}\mathcal{P}_{M,i}\sum_{\ell=1}^{N_r} g_\ell(\mathbf{\Lambda}_r)\left(1+\frac{\gamma\mathcal{E}_{M,i}\lambda_{s,\max}\lambda_{r,\ell}}{4}\right)^{-2}\left(\frac{\gamma\mathcal{E}_{M,i}\lambda_{s,\max}\lambda_{r,\ell}}{4}\right)}} \qquad (35)$$

B. Closed-Form C-PEP Based on Saddlepoint Approximation

The numerator of the saddlepoint approximation (22) for BICM–SM is obtained by evaluating (39) and (40) at the saddlepoint $\hat{s}$, which is easily found to be 1/2. To evaluate the denominator of (22), we require $\mathcal{K}''_{\mathcal{L}}(\hat{s})$. To do this, we start by using (23) and (39) to write

$$\mathcal{K}''_{\mathcal{L}}(\hat{s}) = \frac{\mathcal{M}''_{\mathcal{L}}(\hat{s})}{\mathcal{M}_{\mathcal{L}}(\hat{s})} - \left(\frac{\mathcal{M}'_{\mathcal{L}}(\hat{s})}{\mathcal{M}_{\mathcal{L}}(\hat{s})}\right)^2 \tag{42}$$

where

$$\mathcal{M}'_{\mathcal{L}}(\hat{s}) = \frac{1}{N_t}\sum_{k=1}^{N_t}\sum_{i=1}^{|P_M|}\mathcal{P}_{M,i}\tilde{\mathcal{I}}'_{k,\mathcal{E}_{M,i}}(\hat{s}) \tag{43}$$

$$\mathcal{M}''_{\mathcal{L}}(\hat{s}) = \frac{1}{N_t}\sum_{k=1}^{N_t}\sum_{i=1}^{|P_M|}\mathcal{P}_{M,i}\tilde{\mathcal{I}}''_{k,\mathcal{E}_{M,i}}(\hat{s}). \tag{44}$$

We must now evaluate $\tilde{\mathcal{I}}'(\hat{s})$ and $\tilde{\mathcal{I}}''(\hat{s})$. Unfortunately, it is very difficult to evaluate these derivatives based directly on the form of $\tilde{\mathcal{I}}(s)$ that is given in (40). In the Appendix, we perform significant algebraic manipulations to calculate these derivatives as follows:

$$\begin{aligned}\tilde{\mathcal{I}}'_{k,\mathcal{E}_{M,i}}(\hat{s}) &= 0\\ \tilde{\mathcal{I}}''_{k,\mathcal{E}_{M,i}}(\hat{s}) &= 8\tilde{\mathcal{I}}_{k,\mathcal{E}_{M,i}}(\hat{s})^2\sum_{\ell=1}^{N_r-N_t+1}\ell C_\ell(\mathbf{\Lambda}_r)\left(\frac{\gamma\mathcal{E}_{M,i}}{4[\mathbf{S}^{-1}]_{kk}}\right)^\ell\end{aligned} \tag{45}$$

where $C_\ell(\mathbf{\Lambda}_r)$, for $\ell = 1, \ldots, N_r - N_t + 1$, are auxiliary constants, which are defined in (63). We now substitute (45) into (43) and (44), simplify the resulting expression, and then use (42) and (22) to give the final closed-form C-PEP saddlepoint approximation in (46), shown at the bottom of the page.

1) Special Case—$N_t = 2, N_r = 2$: For 2×2 systems, (46) can be reduced to a simple closed-form expression.[5] We first note that [34]

$$[\mathbf{S}^{-1}]_{kk} = \frac{|\mathbf{S}^{kk}|}{|\mathbf{S}|} \tag{47}$$

[5]Although not shown, simplified expressions are also possible for the more general case $N_r = N_t = n$ and for systems with $N_t = 2$ and $N_r \geq 2$.

where $\mathbf{S}^{kk}$ corresponds to $\mathbf{S}$, with the kth row and column removed, and recall that the spatial correlation matrices have unity diagonal entries, such that, for 2×2 systems

$$[\mathbf{S}^{-1}]_{kk} = \frac{1}{|\mathbf{S}|} \tag{48}$$

for $k = 1, 2$. Second, we note that (46) contains only a single auxiliary constant $C_1(\mathbf{\Lambda}_r)$ in the 2×2 case, in which case, (63) reduces to

$$C_1(\mathbf{\Lambda}_r) = 2|\mathbf{R}|. \tag{49}$$

Substituting (48) and (49) into (46) and simplifying yields

$$f(d,\mu,\mathcal{A},\gamma) \approx \frac{1}{2\sqrt{\pi d}}\frac{\left(\sum_{i=1}^{|\mathcal{P}_M|}\mathcal{P}_{M,i}\left(1+\frac{\gamma\mathcal{E}_{M,i}|\mathbf{R}||\mathbf{S}|}{4}\right)^{-1}\right)^{d+\frac{1}{2}}}{\sqrt{\sum_{i=1}^{|\mathcal{P}_M|}\mathcal{P}_{M,i}\frac{\frac{\gamma\mathcal{E}_{M,i}|\mathbf{R}||\mathbf{S}|}{4}}{\left(1+\frac{\gamma\mathcal{E}_{M,i}|\mathbf{R}||\mathbf{S}|}{4}\right)^2}}}. \tag{50}$$

C. Simplified C-PEP at High SNR

In the high-SNR regime, we note that the summations over ℓ in (46) are dominated by the terms corresponding to $\ell = N_r - N_t + 1$. We also note in the Appendix, from (63), that

$$C_{N_r-N_t+1}(\mathbf{\Lambda}_r) = \binom{N_r}{N_t-1}|\mathbf{R}|. \tag{51}$$

With these observations, after basic algebra, it is easily shown that (46) reduces to

$$\begin{aligned}f(d,\mu,\mathcal{A},\gamma) \approx \left(\frac{\gamma}{4}\right)^{-(N_r-N_t+1)d}&\frac{\mathrm{tr}_{N_t-1}(\mathbf{\Lambda}_r)^d}{2N_t^d\sqrt{\pi d}\binom{N_r}{N_t-1}^d|\mathbf{R}|^d}\\ &\times\left(\sum_{k=1}^{N_t}\sum_{i=1}^{|\mathcal{P}_M|}\mathcal{P}_{M,i}\left(\frac{\mathcal{E}_{M,i}}{[\mathbf{S}^{-1}]_{kk}}\right)^{-(N_r-N_t+1)}\right)^d\end{aligned} \tag{52}$$

which is clearly much simpler than (46).

$$f(d,\mu,\mathcal{A},\gamma) \approx \frac{1}{2N_t^d\sqrt{\pi d}}\frac{\left(\sum_{k=1}^{N_t}\sum_{i=1}^{|\mathcal{P}_M|}\mathcal{P}_{M,i}\left(1+\sum_{\ell=1}^{N_r-N_t+1}\left(\frac{\gamma\mathcal{E}_{M,i}}{4[\mathbf{S}^{-1}]_{kk}}\right)^\ell C_\ell(\mathbf{\Lambda}_r)\right)^{-1}\right)^{d+\frac{1}{2}}}{\sqrt{\sum_{k=1}^{N_t}\sum_{i=1}^{|\mathcal{P}_M|}\mathcal{P}_{M,i}\frac{\sum_{\ell=1}^{N_r-N_t+1}\ell\left(\frac{\gamma\mathcal{E}_{M,i}}{4[\mathbf{S}^{-1}]_{kk}}\right)^\ell C_\ell(\mathbf{\Lambda}_r)}{\left(1+\sum_{\ell=1}^{N_r-N_t+1}\left(\frac{\gamma\mathcal{E}_{M,i}}{4[\mathbf{S}^{-1}]_{kk}}\right)^\ell C_\ell(\mathbf{\Lambda}_r)\right)^2}}}} \tag{46}$$

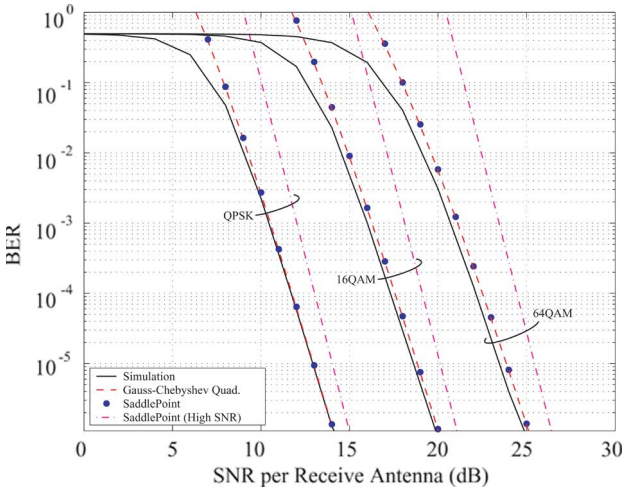

Fig. 4. Simulated and analytical BER 2×2 BICM–SM employing a 1/2-rate code and for various modulation schemes. An exponential correlation model is used, with a correlation coefficient of 0.5 at both the transmitter and receiver.

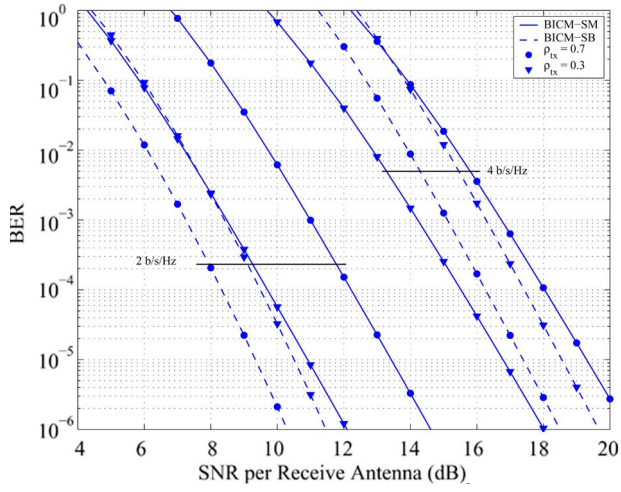

Fig. 5. BER curves based on the tight C-PEP expressions (35) and (50) for 2×2 BICM–SB and BICM–SM, respectively. Two exponential correlated channel scenarios are presented, with $\rho_{\mathrm{rx}} = 0.1$, $\rho_{\mathrm{tx}} = 0.3$, and $\rho_{\mathrm{rx}} = 0.1$, $\rho_{\mathrm{tx}} = 0.7$.

1) Special Case—$N_t = 2$, $N_r = 2$: In this case, (52) reduces to the extremely simple expression

$$f(d, \mu, \mathcal{A}, \gamma) \approx \frac{1}{2\sqrt{\pi d}} \left(\frac{\gamma |\mathbf{R}||\mathbf{S}|}{4} \left(\sum_{i=1}^{|\mathcal{P}_M|} \frac{\mathcal{P}_{M,i}}{\mathcal{E}_{M,i}} \right)^{-1} \right)^{-d}. \tag{53}$$

D. BER Performance Results

Fig. 4 compares the preceding analytical BICM–SM BER expressions with Monte Carlo simulation results, for a 2×2 system with Gray-labeled QPSK, 16QAM, and 64QAM constellations. The same system and channel parameters are assumed as in Section V-D. The "saddlepoint" curves were obtained by substituting the C-PEP expression (50) into (18) and are clearly tight for low to moderate BERs. The "saddlepoint (high SNR)" curves were obtained from (53). We see that these curves tighten as the BER is reduced and are within 1 dB of the simulated curves for BERs below 10^{-6}. For comparison, results are also presented based on the exact C-PEP expression (21), which are obtained using the mgf (39), and GCQ rules for evaluating the complex integration in (21).

VII. SM/SB Switching for Coded MIMO

In this section, we present a novel low-complexity switching strategy for BICM mode and MIMO transmission scheme selection. Our proposed switching strategy is based purely on the analytical results of the previous two sections and does not require any empirically generated lookup tables. The approach is shown to yield significant improvements in system throughput for the transmit and receive correlated Rayleigh channels that we are considering.

A. BER Performance Comparison in Correlated Channels

Before presenting the details of the switching strategy, we first investigate the relative performance of BICM–SB and BICM–SM in various correlation scenarios.

Fig. 5 considers 2×2 fully interleaved systems (achieved using a 564-bit block interleaver [10] and assuming fast fading) and shows BER curves based on the C-PEP expressions (35) for BICM–SB and (50) for BICM–SM, which have previously been shown to be tight. For the 2-bit/s/Hz case, BICM–SB operates with the 1/2-rate code discussed in Section V-D (and used throughout this paper) and 16QAM, and BICM–SM operates with the 1/2-rate code and QPSK. For the 4-bit/s/Hz case, BICM–SB operates with a 2/3-rate code (obtained by puncturing the preceding 1/2-rate code, as outlined in [35]) and 64QAM, whereas BICM–SM operates with the 1/2-rate code and 16QAM.

As expected, we observe that BICM–SM degrades with increasing transmit correlation. In contrast, the BER of BICM–SB *improves* with increasing transmit correlation. This improvement is due to more energy being focused in the direction of the SB vector $\mathbf{u}_{s,\max}$, yielding an SNR gain. The relative performance is, of course, the important factor in designing a switching scheme, and this is highly influenced by the correlation and the spectral efficiency. The figure shows that, for 2 bit/s/Hz, BICM–SB outperforms BICM–SM in both correlation scenarios. At 4 bit/s/Hz, however, BICM–SB is best for $\rho_{\mathrm{tx}} = 0.7$, and BICM–SM is best for $\rho_{\mathrm{tx}} = 0.3$.

Fig. 6 examines in more detail the relative performance of BICM–SB and BICM–SM as a function of transmit correlation. The figure shows the minimum required SNR (or *SNR threshold*) to achieve a BER of 10^{-3} for the 4-bit/s/Hz systems considered in Fig. 5. The curves were evaluated using C-PEP expressions as in Fig. 5. Note that, even if one wanted to, it is infeasible to accurately generate these curves in a practical time frame via simulation since they require inverting the BER versus SNR curves. Hence, our tight efficient analytical expressions are particularly useful here. Results are presented as a function of ρ_{tx}, for three example correlated channels with $\rho_{\mathrm{rx}} = 0.1, 0.5,$ and 0.9. Clearly, the SM scheme requires increasing SNR to achieve the target BER, as the transmit correlation increases. The reverse is true for the SB scheme. The important observation from a switching algorithm point

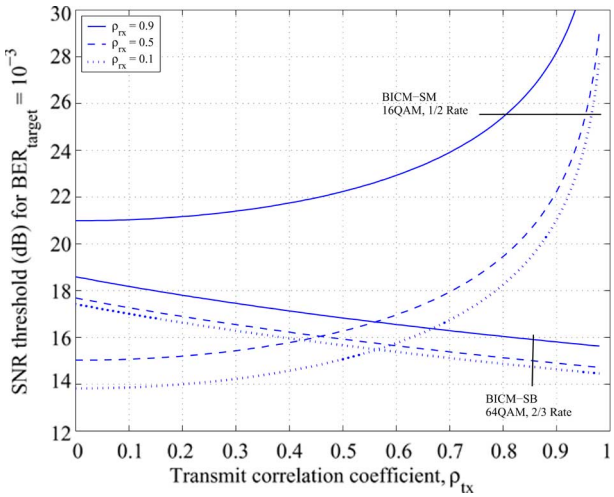

Fig. 6. SNR thresholds corresponding to a target BER of 10^{-3} for BICM–SM and BICM–SB as a function of $\rho_{\rm rx}$ and $\rho_{\rm tx}$. Results are shown for 2×2 BICM–SM with 16QAM and a 1/2-rate code and BICM–SB with 64QAM and a 2/3-rate code.

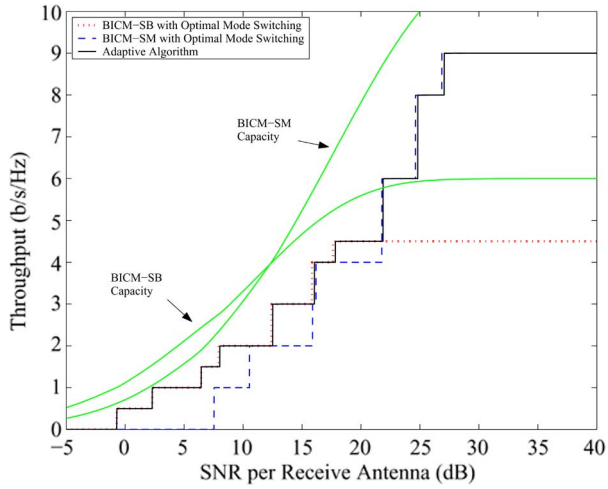

Fig. 7. Throughput achieved by the proposed switching algorithm for a 2×2 system with a target BER of 10^{-3} and for correlated channels with $\rho_{\rm rx} = \rho_{\rm tx} = 0.5$. Mode and transmission scheme selection is based on the tight C-PEP expressions (35) and (50). Throughputs with optimal mode selection and LLC envelope curves are also given.

of view is that the curves can cross. For example, for receive correlation $\rho_{\rm rx} = 0.1$, it is clearly desirable to use BICM–SM for $\rho_{\rm tx} \leq 0.55$ and to use BICM–SB for $\rho_{\rm tx} > 0.55$. Another interesting observation is that both SB and SM are negatively affected by increasing receive correlation. This is particularly significant for SM.

B. Analytical BICM Mode and MIMO Transmission Scheme Selection Algorithm

Clearly, there are significant benefits to be gained from switching between BICM–SM and BICM–SB, depending on the channel correlation and the SNR. We now demonstrate how our new closed-form BER approximations can be used to maximize system throughput while satisfying a predefined BER.

The throughput ν can be calculated for a given BICM mode and MIMO transmission scheme using

$$\nu = S(1 - \text{BER}) \tag{54}$$

where S is the spectral efficiency. For a given mode, the spectral efficiencies are calculated for the SB and SM transmission schemes according to (6) and (7), respectively.

The switching procedure that we consider is given as follows.

- At regular intervals (dependent on the specific application), the receiver estimates the average SNR γ and channel spatial correlation matrices $\mathbf{R}$ and $\mathbf{S}$.
- The receiver then calculates the BER in (18) using (35) for the SB scheme and (46) for the SM scheme for each of the BICM modes (from the set of available modes).
- For all mode-scheme combinations, which satisfy the BER constraint, the receiver calculates the throughput using (54).
- The mode-scheme combination with the highest throughput is then selected. If this combination is different from what is currently being transmitted, then its index is conveyed back to the transmitter (along with the beamforming vector in the case of SB being selected).

Note that the formulas used in this proposed switching procedure are quite straightforward from an implementation point of view. In particular, the BER in (18) can be accurately truncated to only five terms, and the PEP expressions (35) and (46) consist of simple summations (with very few terms), multiplications, and some basic matrix manipulations. We also note that they are presented in this paper in their most general form, and for many practical scenarios, they can be reduced, such as the 2×2 example given explicitly in (50).

We note that similar switching schemes have been proposed for a range of other coding/correlation scenarios (e.g., [4]–[7], [14], and [15]); however, they generally require lookup tables (and are therefore less accurate) or instantaneous channel knowledge, or they do not allow for either coding or double-ended correlation.

C. Throughput Performance Results

In this section, we consider 2×2 systems and employ the eight BICM modes that are defined by the IEEE 802.11a standard in [35]. Note, however, that our algorithm applies equally to any antenna configuration and for any set of modes comprising Gray-labeled modulation formats.

Fig. 7 shows throughput results for a target BER of 10^{-3} and for correlated channels with $\rho_{\rm rx} = \rho_{\rm tx} = 0.5$. The figure shows the throughputs obtained by BICM–SB and BICM–SM with optimal mode switching, where the switching points are calculated based on the actual simulated BER curves. For comparison, LLC envelope curves (as derived in Section III) are also shown. The solid line in the figure corresponds to our proposed switched selection algorithm, where the switching points are based on the tight C-PEP expressions (35) and (50) for BICM–SB and BICM–SM, respectively. Clearly, our switching approach achieves near-optimal throughputs for all SNRs. As expected, BICM–SB is selected for low SNRs, and BICM–SM is selected for high SNRs.

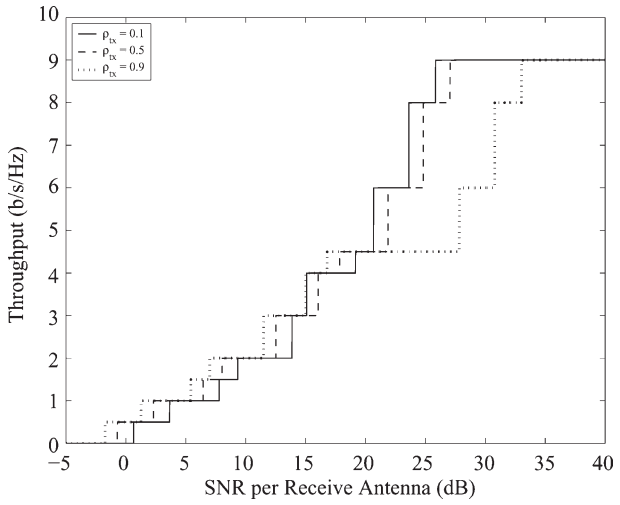

Fig. 8. Throughputs achieved by the proposed switching algorithm for a 2×2 system with a target BER of 10^{-3}, in different exponential correlated channel scenarios, with $\rho_{\mathrm{rx}} = 0.5$ and ρ_{tx} values of 0.1, 0.5, and 0.9. Mode and transmission scheme selection is based on the tight C-PEP expressions (35) and (50).

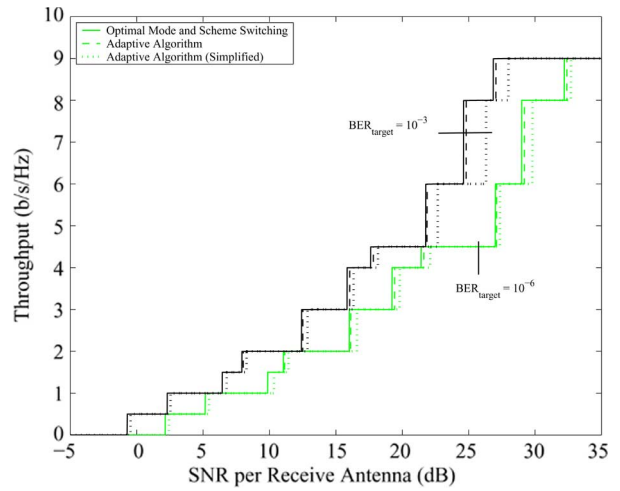

Fig. 9. Throughput comparison of two mode/transmission scheme selection approaches. The first is based on the tight C-PEP expressions (35) and (46); the second is based on the simplified expressions (37) and (52). Results are shown for 2×2 systems with target BERs of 10^{-3} and 10^{-6}, and for channels with $\rho_{\mathrm{rx}} = \rho_{\mathrm{tx}} = 0.5$.

Fig. 8 shows the throughputs of the proposed switching algorithm in various transmit-correlation scenarios. For SNRs below 20 dB, the throughputs improve with increasing transmit correlation since BICM–SB was selected by the switching algorithm in this low-SNR regime. Conversely, for SNRs above 20 dB, the switching algorithm selected BICM–SM, and hence, the throughput degrades with increasing transmit correlation.

Fig. 9 compares the selection algorithm based on the tight C-PEP expressions (35) and (50), with the selection algorithm based on the simplified C-PEP expressions (37) and (53). The figure includes throughput curves corresponding to optimal switching based on actual simulated BERs. We see that, for a target BER of 10^{-3}, both algorithms perform very close to the optimal curve for SNRs ≤ 20 dB. For SNRs above this, the simplified algorithm incurs a noticeable loss. At the lower target BER of 10^{-6}, the simplified algorithm performs close to the optimal curves for *all* SNRs. This is because, in this region, the SM scheme is chosen, and the C-PEP expression (53) is tighter at this target BER, in comparison to 10^{-3}, as seen in Fig. 4. This yields more accurate SNR thresholds for all BICM–SM modes, thereby improving the throughput achieved by the simplified algorithm when these modes are employed (i.e., in the high-SNR regime).

VIII. Conclusion

We have shown that significant throughput gains can be achieved by optimizing the choice of code rate, modulation format, and MIMO transmission scheme in spatially correlated channels. We presented a novel practical switching algorithm for low-complexity coded-MIMO transmission based on new closed-form approximations to the BER. The proposed approach has minimal feedback requirements and provides significant throughput enhancements for fixed target error rate over nonswitching methods.

Appendix

Derivation of (45)

To calculate $\tilde{\mathcal{I}}'(\cdot)$ and $\tilde{\mathcal{I}}''(\cdot)$, we manipulate $\tilde{\mathcal{I}}(\cdot)$ in (40) as follows: We first express the inverse in the denominator of (40) as[6]

$$[\mathbf{I}_{N_r} + K_{k,i}(s)\mathbf{\Lambda}_r]^{-1} = \mathrm{diag}\left(\frac{1}{1 + K_{k,i}(s)\lambda_{r,q}}\right) \tag{55}$$

where, for convenience, we have defined

$$K_{k,i}(s) \triangleq \frac{\gamma \mathcal{E}_{M,i} s(1-s)}{[\mathbf{S}^{-1}]_{k,k}}. \tag{56}$$

We also write the determinant in (40) as

$$|\mathbf{I}_{N_r} + K_{k,i}(s)\mathbf{\Lambda}_r| = \prod_{j=1}^{N_r} (1 + K_{k,i}(s)\lambda_{r,j}). \tag{57}$$

Using (55) and (57), it can be shown that

$$\tilde{\mathcal{I}}_{k,\mathcal{E}_{M,i}}(s) = \frac{\mathrm{tr}_{N_t-1}(\mathbf{\Lambda}_r)}{\mathrm{tr}_{N_t-1}\left(\mathrm{diag}\left(\frac{\lambda_{r,q}}{1+K_{k,i}(s)\lambda_{r,q}}\right)\right)} \times \frac{1}{\prod_{j=1}^{N_r}(1 + K_{k,i}(s)\lambda_{r,j})}. \tag{58}$$

We now focus on the denominator in (58), which we assign the function name $D(s)$. The key here is to express $D(s)$ as a polynomial in $K_{k,i}(s)$, which will then allow the required

[6]Here, we introduce a compact notation to represent the diagonal matrix in terms of the qth diagonal element.

derivatives to be evaluated. Expanding the esf according to (41) gives

$$D(s) = \mathrm{tr}_{N_t-1}\left(\mathrm{diag}\left(\frac{\lambda_{r,q}}{1+K_{k,i}(s)\lambda_{r,q}}\right)\right)\prod_{j=1}^{N_r}(1+K_{k,i}(s)\lambda_{r,j})$$
$$= \left(\sum_{\{\underline{\alpha}\}}\prod_{j=1}^{N_t-1}\left(\frac{\lambda_{r,\alpha_j}}{1+\lambda_{r,\alpha_j}}\right)\right)\prod_{j=1}^{N_r}(1+K_{k,i}(s)\lambda_{r,j})$$
$$= \sum_{\{\underline{\alpha}\}}\prod_{j=1}^{N_t-1}\lambda_{r,\alpha_j}\left(\prod_{j=1}^{N_r-N_t+1}\left(1+K_{k,i}(s)\lambda_{r,\beta_j}\right)\right) \quad (59)$$

where $\{\beta_1,\ldots,\beta_{N_r-N_t+1}\} = \{1,\ldots,N_r\}\setminus\underline{\alpha}$. In order to obtain a polynomial expression, we use the following generating function expansion [36]:

$$\prod_{q=1}^{N}(1+ax_q) = 1+\sum_{\ell=1}^{N}a^\ell\,\mathrm{tr}_\ell\left(\mathrm{diag}(x_q)\right) \quad (60)$$

which gives

$$D(s) = \mathrm{tr}_{N_t-1}(\mathbf{\Lambda}_r) + \sum_{\ell=1}^{N_r-N_t+1}K_{k,i}(s)^\ell \times\sum_{\{\underline{\alpha}\}}\left(\prod_{j=1}^{N_t-1}\lambda_{r,\alpha_j}\right)\mathrm{tr}_\ell\left(\mathrm{diag}(\lambda_{r,\beta_q})\right). \quad (61)$$

Finally, substituting $D(s)$ as the denominator in (58), we obtain the simplified expression

$$\tilde{\mathcal{I}}_{k,\mathcal{E}_{M,i}}(s) = \left(1+\sum_{\ell=1}^{N_r-N_t+1}K_{k,i}(s)^\ell C_\ell(\mathbf{\Lambda}_r)\right)^{-1} \quad (62)$$

where we have defined the auxiliary constants

$$C_\ell(\mathbf{\Lambda}_r) \triangleq \sum_{\{\underline{\alpha}\}}\left(\prod_{j=1}^{N_t-1}\lambda_{r,\alpha_j}\right)\mathrm{tr}_\ell\left(\mathrm{diag}(\lambda_{r,\beta_q})\right) \quad (63)$$

for $\ell = 1,\ldots,N_r-N_t+1$. Now, using (62), we easily evaluate $\tilde{\mathcal{I}}'_{k,\mathcal{E}_{M,i}}(\hat{s})$ and $\tilde{\mathcal{I}}''_{k,\mathcal{E}_{M,i}}(\hat{s})$ and perform some simple algebra to obtain the desired result.

REFERENCES

[1] İ. E. Telatar, "Capacity of multi-antenna Gaussian channels," *Eur. Trans. Commun.*, vol. 10, no. 6, pp. 585–595, Nov./Dec. 1999.

[2] V. Tarokh, N. Seshadri, and R. Calderbank, "Space-time codes for high data rate wireless communication: Performance criterion and code construction," *IEEE Trans. Inf. Theory*, vol. 44, no. 2, pp. 744–765, Mar. 1998.

[3] L. Zheng and D. N. C. Tse, "Diversity and multiplexing: A fundamental tradeoff in multiple-antenna channels," *IEEE Trans. Inf. Theory*, vol. 49, no. 5, pp. 1073–1096, May 2003.

[4] R. W. Heath, Jr. and A. Paulraj, "Switching between multiplexing and diversity based on constellation distance," in *Proc. Allerton Conf. Commun., Control, Comput.*, Sep. 2000.

[5] R. W. Heath, Jr. and D. J. Love, "Multi-mode antenna selection for spatial multiplexing systems with linear receivers," in *Proc. Allerton Conf. Commun., Control, Comput.*, Monticello, IL, Oct. 2003.

[6] R. Narasimhan, "Spatial multiplexing with transmit antenna and constellation selection for correlated MIMO fading channels," *IEEE Trans. Signal Process.*, vol. 51, no. 11, pp. 2829–2838, Nov. 2003.

[7] S. Catreux, V. Erceg, D. Gesbert, and R. W. Heath, Jr., "Adaptive modulation and MIMO coding for broadband wireless data networks," *IEEE Commun. Mag.*, vol. 40, no. 6, pp. 108–115, Jun. 2002.

[8] E. Zehavi, "8-PSK trellis codes for a Rayleigh channel," *IEEE Trans. Commun.*, vol. 40, no. 5, pp. 873–884, May 1992.

[9] G. Caire, G. Taricco, and E. Biglieri, "Bit-interleaved coded modulation," *IEEE Trans. Inf. Theory*, vol. 44, no. 3, pp. 927–946, May 1998.

[10] M. R. G. Butler and I. B. Collings, "A zero-forcing approximate log-likelihood receiver for MIMO bit-interleaved coded modulation," *IEEE Commun. Lett.*, vol. 8, no. 2, pp. 105–107, Feb. 2004.

[11] M. R. McKay and I. B. Collings, "Capacity and performance of MIMO-BICM with zero forcing receivers," *IEEE Trans. Commun.*, vol. 53, no. 1, pp. 74–83, Jan. 2005.

[12] A. Martinez, A. Guillén i Fàbregas, and G. Caire, "New simple evaluation of the error probability of bit-interleaved coded modulation using the saddlepoint approximation," in *Proc. ISITA*, Parma, Italy, Oct. 2004.

[13] A. Martinez, A. Guillén i Fàbregas, and G. Caire, "Error probability analysis of bit-interleaved coded modulation," *IEEE Trans. Inf. Theory*, vol. 52, no. 1, pp. 262–271, Jan. 2006.

[14] A. Forenza, A. Pandharipande, H. Kim, and R. W. Heath, Jr., "Adaptive MIMO transmission scheme: Exploiting the spatial selectivity of wireless channels," in *Proc. IEEE VTC*, Stockholm, Sweden, May 2005, pp. 3188–3192.

[15] A. Forenza, M. R. McKay, A. Pandharipande, R. W. Heath, Jr., and I. B. Collings, "Capacity enhancement via multi-mode adaptation in spatially correlated MIMO channels," in *Proc. IEEE Int. Symp. PIMRC*, Berlin, Germany, Sep. 2005, pp. 754–758.

[16] E. A. Jorswieck and H. Boche, "Channel capacity and capacity-range of beamforming in MIMO wireless systems under correlated fading with covariance feedback," *IEEE Trans. Wireless Commun.*, vol. 3, no. 5, pp. 1543–1553, Sep. 2004.

[17] M. Kiessling and J. Speidel, "Mutual information of MIMO channels in correlated Rayleigh fading environments—A general solution," in *Proc. IEEE ICC*, Paris, France, Jun. 2004, pp. 814–818.

[18] M. R. McKay and I. B. Collings, "General capacity bounds for spatially correlated Rician MIMO channels," *IEEE Trans. Inf. Theory*, vol. 51, no. 9, pp. 3121–3145, Sep. 2005.

[19] G. J. Foschini, "Layered space-time architecture for wireless communications in a fading environment when using multi-element antennas," *Bell Lab. Tech. J.*, vol. 1, no. 2, pp. 41–59, Autumn 1996.

[20] M. Abramowitz and I. A. Stegun, *Handbook of Mathematical Functions With Formulas, Graphs, and Mathematical Tables*, 9th ed. New York: Dover, 1970.

[21] D. Gore, R. W. Heath, Jr., and A. Paulraj, "Transmit selection in spatial multiplexing systems," *IEEE Commun. Lett.*, vol. 6, no. 11, pp. 491–493, Nov. 2002.

[22] D. Divsalar, H. Jin, and R. J. McEliece, "Coding theorems for 'turbo-like' codes," in *Proc. Allerton Conf. Commun., Control, Comput.*, Monticello, IL, Sep. 1998, pp. 201–210.

[23] X. Li and J. A. Ritcey, "Trellis-coded modulation with bit interleaving and iterative decoding," *IEEE J. Sel. Areas Commun.*, vol. 17, no. 4, pp. 715–724, Apr. 1999.

[24] X. Li, A. Chindapol, and J. A. Ritcey, "Bit-interleaved coded modulation with iterative decoding and 8PSK signalling," *IEEE Trans. Commun.*, vol. 50, no. 8, pp. 1250–1257, Aug. 2002.

[25] A. M. Tonello, "Space-time bit-interleaved coded modulation with an iterative decoding strategy," in *Proc. IEEE VTC*, Boston, MA, Sep. 2000, pp. 473–478.

[26] A. J. Viterbi and J. K. Omura, *Principles of Digital Communication and Coding*. New York: McGraw-Hill, 1979.

[27] R. Gallager, *Information Theory and Reliable Communication*. Hoboken, NJ: Wiley, 1968.

[28] R. Durrett, *Probability: Theory and Examples*, 2nd ed. Belmont, CA: Duxbury, 1996.

[29] A. M. Mathai and S. B. Provost, *Quadratic Forms in Random Variables*. New York: Marcel Dekker, 1992.

[30] I. S. Gradshteyn and I. M. Ryzhik, *Table of Integrals, Series, and Products*, 4th ed. San Diego, CA: Academic, 1965.

[31] M. R. McKay and I. B. Collings, "Error performance of MIMO-BICM with zero-forcing receivers in spatially-correlated Rayleigh channels," *IEEE Trans. Wireless Commun.*, vol. 6, no. 3, pp. 787–792, Mar. 2007.

[32] E. Biglieri, G. Caire, G. Taricco, and J. Ventura-Traveset, "Simple method for evaluating error probabilities," *Electron. Lett.*, vol. 32, no. 3, pp. 191–192, Feb. 1996.

[33] A. W. Marshall and I. Olkin, *Inequalities: Theory of Majorization and Its Applications*. New York: Academic, 1979.
[34] R. A. Horn and C. R. Johnson, *Matrix Analysis*, 4th ed. New York: Cambridge Univ. Press, 1990.
[35] IEEE 802.11, *Supplement to IEEE Standard for Telecommunications and Information Exchange Between Systems—LAN and MAN Specific Requirements—Part 11: Wireless LAN MAC and PHY Specifications: High-Speed Physical Layer in the 5 GHz Band,* IEEE Std 802.11a-1999, Sep. 1999.
[36] A. B. Balantekin, "Character expansions, Itzykson-Zuber integrals, and the QCD partition function," *Phys. Rev. D, Part. Fields*, vol. 62, no. 8, pp. 085 017(1)–085 017(8), Sep. 2000.

Matthew R. McKay (S'03–M'06) received the combined B.E. degree in electrical engineering and the B.IT. degree in computer science from the Queensland University of Technology, Brisbane, Australia, in 2002 and the Ph.D. degree in electrical engineering from the University of Sydney, Sydney, Australia, in 2006.

He was a Research Scientist at the Commonwealth Science and Industrial Research Organization (CSIRO), Sydney, prior to joining the faculty of the Hong Kong University of Science and Technology (HKUST), Clear Water Bay, Hong Kong, in 2007, where he is currently an Assistant Professor. He is also a member of the Center for Wireless Information Technology at HKUST. His research interests include the analysis and design of MIMO systems, random matrix theory, information theory, and wireless *ad hoc* and sensor networks.

Iain B. Collings (S'92–M'95–SM'02) was born in Melbourne, Australia, in 1970. He received the B.E. degree in electrical and electronic engineering from the University of Melbourne in 1992 and the Ph.D. degree in systems engineering from Australian National University, Canberra, Australia, in 1995.

He is currently a Science Leader with the Wireless Technologies Laboratory, Information and Communication Technologies Centre, Commonwealth Scientific and Industrial Research Organisation, Marsfield, Australia. Prior to this, he was an Associate Professor with the University of Sydney, Sydney, Australia (1999–2005), a Lecturer with the University of Melbourne (1996–1999), and a Research Fellow with the Australian Cooperative Research Centre for Sensor Signal and Information Processing (1995). He has published more than 100 research papers in the area of mobile digital communications and, more specifically, channel estimation, equalization, and multicarrier modulation, for time-varying, multiuser, and MIMO channels.

Dr. Collings currently serves as an Editor for the IEEE TRANSACTIONS ON WIRELESS COMMUNICATIONS and as a Guest Editor for the *EURASIP Journal on Advanced Signal Processing*. He has also served as the Vice Chair of the Technical Program Committee for the IEEE Vehicular Technology Conference (Spring) 2006 and has been serving on a number of other TPCs and organizing committees of IEEE conferences. He is also a Founding Organizer of the Australian Communication Theory Workshops 2000–2006.

Antonio Forenza (S'04–M'06) received the M.S. degree in telecommunications engineering from Politecnico di Torino, Torino, Italy, and the Eurecom Institute, Sophia Antipolis, France, in 2001 and the Ph.D. degree in electrical and computer engineering from the University of Texas, Austin, in 2006.

In 2001, he interned as a Systems Engineer at Iospan Wireless, Inc., San Jose, CA— a startup company that developed the first commercial MIMO–OFDM communication system. His main research focus was on link-adaptation and physical layer algorithm design. In the fall of 2001, he joined ArrayComm, Inc., San Jose, as a Systems Research Engineer. At ArrayComm, he was actively involved in the design and implementation of smart antenna systems for the 3G WCDMA wireless platform. Over the summers of 2004 and 2005, he interned as a Research Engineer at Samsung Advanced Institute of Technology, Suwon, Korea, and Freescale Semiconductor, Inc., Austin, TX, respectively, developing adaptive MIMO transmission and MU-MIMO precoding techniques for 3GPP, IEEE 802.11n, and IEEE 802.16e standards systems. Since June 2006, he has been with Rearden, LLC, San Francisco, CA, as a Senior Systems Engineer. His research interests include MIMO antenna design, adaptive MIMO transmission techniques, precoding methods for MU-MIMO, and smart antenna signal processing.

Robert W. Heath, Jr. (S'96–M'01–SM'06) received the B.S. and M.S. degrees from the University of Virginia, Charlottesville, in 1996 and 1997, respectively, and the Ph.D. degree from Stanford University, Stanford, CA, in 2002, all in electrical engineering.

From 1998 to 2001, he was a Senior Member of Technical Staff and then a Senior Consultant with Iospan Wireless Inc., San Jose, CA, where he worked on the design and implementation of the physical and link layers of the first commercial MIMO–OFDM communication system. In 2003, he founded MIMO Wireless Inc.—a consulting company dedicated to the advancement of MIMO technology. Since January 2002, he has been with the Department of Electrical and Computer Engineering, University of Texas at Austin, where he is currently an Associate Professor and a member of the Wireless Networking and Communications Group. His research interests cover a broad range of MIMO communication including limited feedback techniques, antenna design, practical receiver architectures, multihop networks, and scheduling algorithms, as well as 60-GHz communication techniques.

Dr. Heath serves as an Editor for the IEEE TRANSACTIONS ON COMMUNICATIONS, an Associate Editor for the IEEE TRANSACTIONS ON VEHICULAR TECHNOLOGY, and a member of the Signal Processing for Communications Technical Committee of the IEEE Signal Processing Society.